

EFFECT OF PRINTING PARAMETERS AND POST-CURING ON MECHANICAL PROPERTIES OF PHOTOPOLYMER PARTS FABRICATED VIA 3D STEREOLITHOGRAPHY PRINTING

RAFFLE RAED DIAB, ABASS ENZI AND OMAR HASHIM HASSOON

*Department of Production Engineering and Metallurgy,
University of Technology, Baghdad, Iraq*

**Corresponding author: Abass.M.Jabber@uotechnology.edu.iq*

(Received: 4 March 2023; Accepted: 22 May 2023; Published on-line: 4 July 2023)

ABSTRACT: Three-dimensional printing has recently come into the spotlight due to its promising potential to create physically three-dimensional parts or structures through computer-aided design. While there are many options for 3D printing methods, photopolymerization 3D printing has garnered much attention because of its high resolution. However, the mechanical properties of photopolymerized 3D printed parts can vary widely depending on the manufacturing parameters and post-processing settings used. This research focuses on studying the effect of printing variables on the mechanical properties of samples printed using a Stereolithography machine (Formlabs, Form+3). Three variables are used: layer thickness (25 and 50 μm), part orientation (X and Z directions), and post-curing. Also, eight groups of 3D-printed photopolymer specimens for twenty-four specimens are used for the tensile test results. The results showed the printing variables affected the mechanical properties of samples, which were proven by Young's modulus, ultimate stress, and ultimate strain.

ABSTRAK: Pencetakan tiga dimensi baru-baru ini menjadi perhatian kerana potensinya yang menjanjikan bagi mencipta bahagian atau struktur tiga dimensi secara fizikal melalui reka bentuk bantuan komputer. Walaupun terdapat banyak pilihan bagi kaedah pencetakan 3D, pencetakan 3D fotopolimerisasi telah mendapat banyak perhatian kerana resolusinya yang tinggi. Walau bagaimanapun, sifat mekanikal bahagian bercetak 3D fotopolimer adalah pelbagai bergantung pada parameter pembuatan dan tetapan pasca pemrosesan yang digunakan. Kajian ini memberi tumpuan kepada kesan pembolehubah cetakan terhadap sifat mekanikal sampel yang dicetak menggunakan mesin Stereolitografi (Formlabs, Form+3). Tiga pembolehubah digunakan: ketebalan lapisan (25 dan 50 μm), orientasi bahagian (arah X dan Z), dan pasca pengawetan. Juga, lapan kumpulan spesimen fotopolimer cetakan 3D untuk dua puluh empat spesimen digunakan bagi mendapatkan keputusan ujian tegangan. Dapatan kajian menunjukkan pembolehubah cetakan mempengaruhi sifat mekanikal sampel, dibuktikan oleh modulus Young, tegangan utama, dan tarikan utama.

KEYWORDS: *additive manufacturing; stereolithography; photocurable polymer; mechanical properties; post-curing*

1. INTRODUCTION

3D printing is one of the modern manufacturing methods that are gaining popularity because of the possibility of its use in various fields of engineering, medicine, and more. Compared to other manufacturing methods, simple and complex parts can be easily

manufactured in record time using 3D printing. Also, the manufacturing process' waste and its cost are very limited in the printing process, which reduces the manufacturing cost [1]. According to the annual growth rate, 3D printing industry sales in 2020 reached more than 8 billion dollars in sales, equivalent to 14%. In 2013, the worldwide demand for 3D printing materials reached about 2 tons, which is anticipated to grow due to the increased use of printed products [2]. Operating 3D printers and manufacturing is simple; anyone can efficiently handle the machines and manufacture parts. The manufacturing process begins with drawing the 3D part with one of the engineering drawing programs, such as SolidWorks. Then the drawing is saved in STL file format. After that, the file is sent to the 3D printer to start the manufacturing process layer-by-layer after the required manufacturing process parameters are determined [3-7]. As shown in Fig. 1, stereolithography is one of the most important methods of producing 3D parts with good quality. SLA system uses a laser to polymerize a liquid resin and transform it into a solid part by a process called photopolymerization [8,9]. Printing thinner layers results in more cohesion and higher mechanical properties, but it does so at the expense of increased construction time [10]. Layers in Stereolithography are kept in a semi-reacted "green state" with polymerizable groups between them because the polymerization reaction is incomplete, and that helps with layer-to-layer bonding by supplying layers for subsequent polymerization. At the same time, post-curing procedures are used to finish the reaction and covalently bind successive layers. After curing, UV is typically employed to complete polymerization by activating photoinitiators [11].

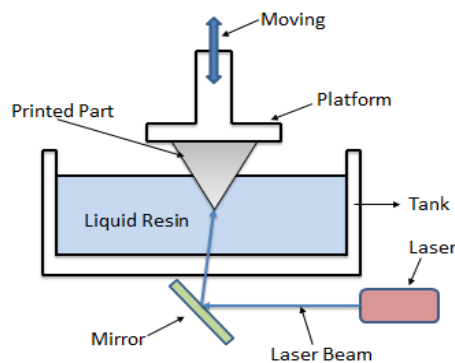


Fig. 1: Scheme of Stereolithography 3D printer machine.

Researchers used an SLA printer in previous work to produce samples with a wide range of print orientations and layer thicknesses [12]. Aznarte et al. [13] examined how 3D printing variables affect the final mechanical properties of specimens created using Digital Light Processing (DLP) 3D printing. Design, printing, and testing in this research were done on several ISO-compliant tensile test specimens. The effect of variables (layer thickness, exposure time, and part orientation) was examined for the elastic modulus, ultimate strain, ultimate tensile strength, and printing time, along with the economic impact of the researched factors regarding printing time. Results presented design guidelines for Vat Photopolymerization procedures. Khalid et al. [14] used the PR 48 photopolymer samples in this investigation using the FORM 2 SLA printer. The elastic modulus and hardness of printed specimens with 50 and 100 μm resolutions were evaluated employing a nanoindentation testing machine at 0° , 45° , and 90° directions. UV was used to cure the samples, and the impact of UV curing duration was examined. Results demonstrated that the elastic modulus and hardness for 100 μm print resolution and 0° orientation was greater if compared to 45° and 90° orientation by 35% and 390%, respectively. Elastic modulus and

hardness for 0° direction were greater than 45° direction by 106%, and greater also for 90° orientation by 92% for 50 µm print resolution. The findings demonstrated that mechanical properties strongly depended on resolution, print direction, and UV curing time. Agrawal [15] attempted to determine which orientation angle is best for which kinds of loads, specifically the fracture test and the dynamic mechanical analysis (DMA) test. Various mechanical property values were obtained during the inspection process. Results showed the orientation angle had a significant impact on the examination process. An average of three samples were taken for each test to reduce the error. After considering the stress-strain and load-extension graphs, the researcher concluded that the orientation angle should be 0°.

The parts manufactured using the SLA system change their mechanical properties according to the selected variables of the printing process. Therefore, some printed samples have poor mechanical properties due to the values of the used printing process variables, as the printing process variables have a significant impact on the mechanical properties of the produced samples. Therefore, the work aim is to determine the effect of part orientation in the X and Z axes, layer thicknesses of 25 and 50 µm, and post-curing on the mechanical properties of printed samples that are fabricated using the SLA system. The specimens' elastic modulus, ultimate stress, and ultimate strain are evaluated and analyzed depending on tensile test results to recognize the variables' values that affect printed specimens' mechanical properties.

2. MATERIAL AND EXPERIMENTAL DETAILS

A detailed description presents the manufacturing process and sample preparation, where the material used in the printing process is explained, as well as the variables of the printing process, the preparation of the number of experiments that are completed, the preparation of samples, and the examination process for samples that are produced through the printing process by a tensile test device.

2.1 Material

Clear resin is ideal for fluidics and mold making, optics, lighting, and any component needing translucency or displaying internal characteristics. It possesses several crucial characteristics, including quality. Formlabs' precisely crafted clear resin captures a model's finest features. Formlabs clear resin is excellent for quick prototyping and product development because it produces accurate, durable pieces, a glossy appearance, and the surface finish of the printed parts is smooth [15]. In the present investigation, specimens are printed with photocurable acrylic-based resin FLGPCL4 (Formlabs, MA, USA).

2.2 Process Parameters

3D printing is one of the basic methods for producing prototype parts. Still, 3D printing is not considered one of the mass production methods due to the long production time, anisotropy, etc. In addition, some critical issues face the 3D printing process, including accuracy, curvature, anisotropy, and the formation of voids inside the manufactured parts. The properties of 3D printed parts are dependent on printing parameters such as temperature, 3D printer machine resolution, layer thickness, geometries, and printing orientations. Therefore, one of the important points before the printing process is to focus on choosing the best process variables for printing to avoid defects in the manufactured parts [7,16-20]. In the current experimental study, there are three process parameters used. Two printing parameters include layer thickness and part orientation, and the third parameter is post-curing. The layer thickness is one of the most critical variables of the printing process, which affects the quality of the produced surface and the mechanical properties of the

manufactured parts. Increasing or decreasing the layer thickness affects the sample's strength. There are many directions for printing, and researchers focus on changing the direction of printing during the sample preparation process to obtain the best quality of the manufactured parts. Part orientation is one of the most studied manufacturing characteristics. Therefore, printing direction statistically impacts the mechanical properties of SLA 3D-printed parts [21-23]. Figure 2 shows the part's orientation for both the X-axis and Z-axis.

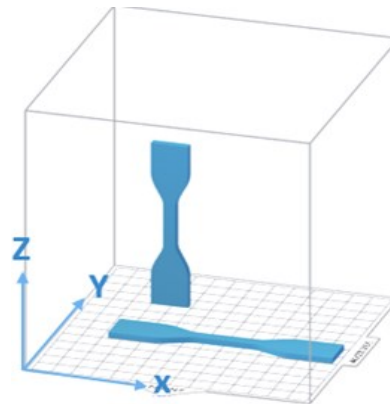


Fig. 2: Printing process directions.

Finishing, including washing and post-curing, are necessary when using SLA printing because areas of uncured resin, whether between layers or on the surface, are considered weak points and damage the material's mechanical properties. The UV post-curing of SLA printed resin can significantly improve the mechanical strength due to the complete curing of any leftover resin.

In addition, the most significant improvement in properties occurs when the UV light is at the same wavelength that the SLA printer uses to cure the resin, as each resin type has a specific wavelength for the curing process. Therefore, the appropriate wavelength must be chosen to cure the resin for the best results [24]. Immediately following the completion of the printing process, the supporting material is removed from the printed part and the part is soaked in isopropyl alcohol for 15 minutes. Alcohol liquefies any uncured resin and cleans the surface of the components. Before testing, materials were allowed to dry for 24 hours on a clean surface. Post-curing is carried out for 50 minutes in a UV chamber, previously heated to 60 °C with a light source of 405 nm and 1.25 mW/cm, see Fig. 3.



Fig. 3: Tensile test specimens during the post-curing process in Formlabs UV chamber (Formcure).

2.3 Experimental Design

SLA technology generates 3D printed parts from a liquid (photopolymer) resin by employing a UV-light source to solidify the liquid substance (resin). To construct a 3D-printed object, a build platform is submerged in a tank of photosensitive thermoset polymeric resin. Once the build platform is submerged, a UV light within the machine solidifies the material by mapping each layer of the object through the tank's bottom. After the light source has printed the layer, the platform rises to allow the swiping blade to apply a fresh coating of resin to the surface; this is continued layer-by-layer until the desired object is created [25]. Table 1 represents all experimental variables and groups that will be used to print the specimens, to ensure that the results of the studies can be reliably replicated; each sample is printed three times.

Table 1: Eight groups (A-H) of specimens with printing parameters

	Symbol	A	B	C	D	E	F	G	H
Variables	Layer thickness (µm)	25	25	25	25	50	50	50	50
	Part orientation	X-axis	X-axis	Z-axis	Z-axis	X-axis	X-axis	Z-axis	Z-axis
	Post-curing	Green	Post-cured	Green	Post-cured	Green	Post-cured	Green	Post-cured

2.3.1 Specimen Preparation

SolidWorks is used to make the 3D model of the specimens following ASTM D638 type IV. Fig. 4 displays the ASTM-required dimensions of the specimen. Slicing can build the model using any CAD software and export it in a 3D printable file format (STL). Each SLA printer includes software to configure printing settings and split the digital model into layers for printing. Once the part design is completed, the print preparation software transmits the instructions to the printer over a wireless or wired connection. For slicing, STL file software named Formlabs preform (Version 3.27.1) is used to slice the specimen into some layers. In addition, the factors are fed to printer software based on the process parameters used in this research.

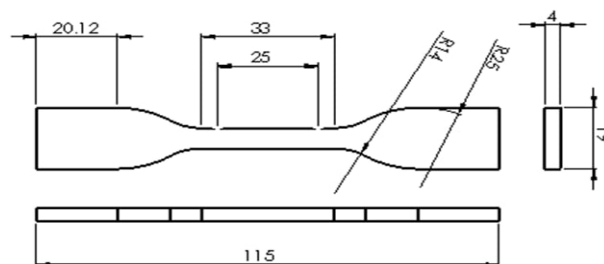


Fig. 4: Standard specimens according to ASTM D638 specimen dimensions (All units in mm) [26].

An SLA machine (Formlabs, Form+3) is used in this research to produce the specimens. Form+3 has a 50 µm resolution in the plane parallel to the printing surface (XY resolution) and a 10 µm resolution perpendicular to the printing surface (Z resolution). Figure 5 depicts

the machine and the necessary support structure for building the specimens in all directions. It was reported that the printer's maximum build dimensions were 145 x 145 x 185 mm.

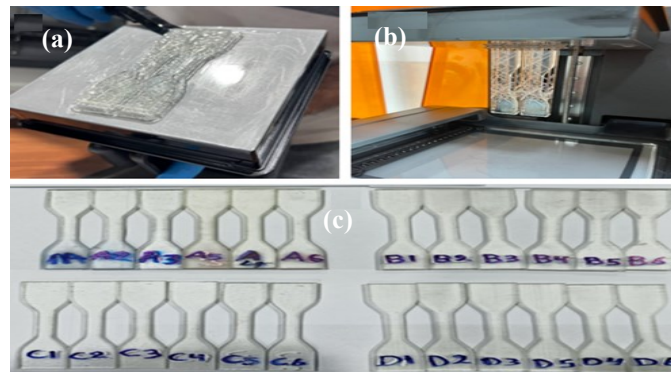


Fig. 5: Fabrication of tensile specimen (a) Longitudinal direction (b) Vertical direction (c) Twenty-four specimens.

2.3.2 Tensile Testing

A Gester universal tensile testing machine is used to test the properties of the printed specimens, with a load cell capacity of 5kN with a crosshead speed of 1mm/min; see Fig. 6.

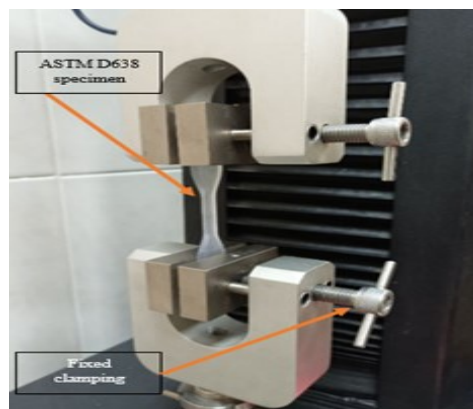


Fig. 6: Specimen placed inside the grips of the Gester universal tensile testing machine.

3. RESULTS AND DISCUSSION

In this section, the tensile test results are shown and discussed. The section is separated into three subsections that discuss the effect of several elements on Young's modulus, ultimate stress, and ultimate strain, respectively. Table 2 shows eight specimens for twenty-four groups representing a variety of process parameters.

Figure 7 shows the relationship between displacement (mm) and force (N) for green and cured samples. The curing process and layer thickness increased the tensile strength of the samples, taking into account the printing orientation. The cured samples had greater tensile strength than the green samples with decreased displacement because the material's behavior tends towards the sample's fragility. However, the green samples had more significant displacement than the cured samples. The tensile strength and displacement values change according to the printing variables, which indicate that the variables significantly impact tensile strength.

Table 2: Tensile testing results for twenty-four specimens depending on the printing parameters and post-curing

Sample	Young's modulus E (MPa)	Average of modulus E (MPa)	Ultimate stress (MPa)	Average of ultimate stress (MPa)	Strain at break (Xf)	Average of strain at break (Xf)
A1	1394.6		46.019		0.109	
A2	1135.883	1301.961	43.956	44.892	0.099	0.108
A3	1375.4		44.700		0.116	
B1	1626.75		61.8238		0.085	
B2	1659.25	1648.417	55.423	57.5566	0.0522	0.073067
B3	1659.25		55.423		0.082	
C1	1339.273		48.248		0.085	
C2	1336.182	1326.479	47.766	49.217	0.104	0.106
C3	1303.983		51.638		0.13	
D1	1818.5		62.193		0.067	
D2	1784.75	1767.274	62.112	61.707	0.066	0.067333
D3	1698.571		60.815		0.069	
E1	619.564		35.097		0.0635	
E2	916.933	796.141	35.416	33.159	0.049	0.0822
E3	851.925		28.963		0.134	
F1	1526		56.990		0.057	
F2	1347.8	1487.119	54.248	57.307	0.076	0.064
F3	1587.556		60.684		0.059	
G1	1236.167		41.537		0.076	
G2	1309.333	1228.141	44.778	42.219	0.113	0.103333
G3	1138.923		40.342		0.121	
H1	1794.5		61.731		0.0625	
H2	1449.6	1699.033	59.433	60.277	0.118	0.0815
H3	1853		59.666		0.064	

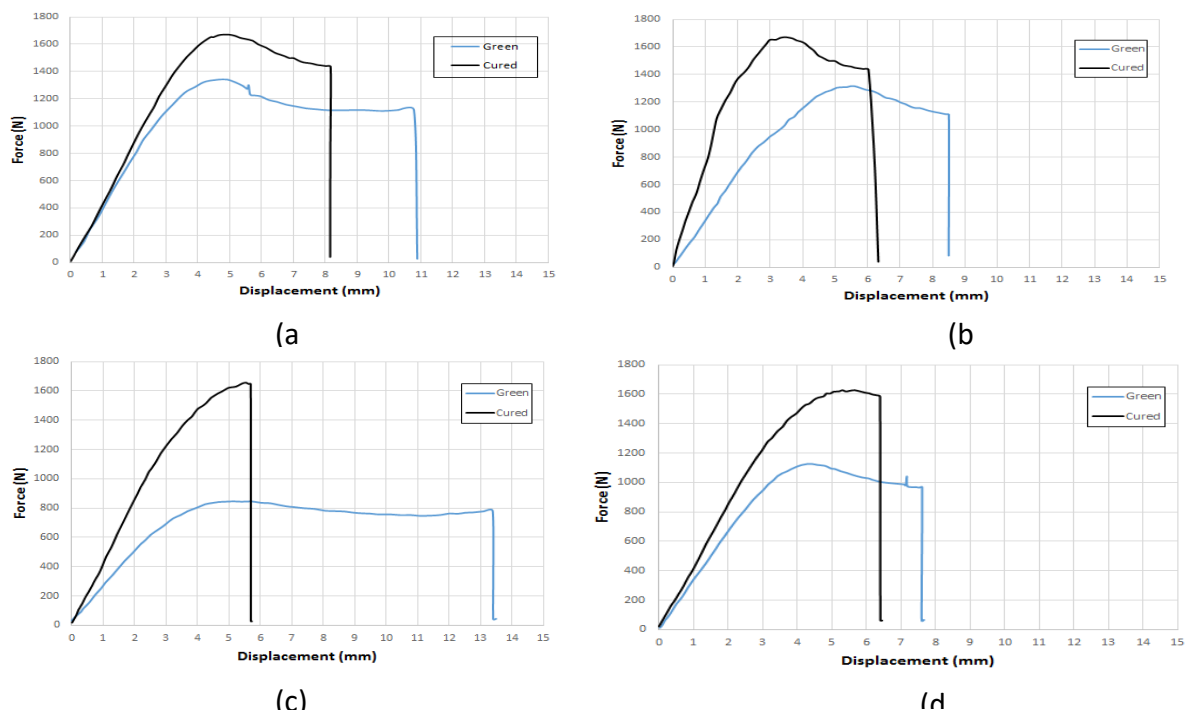


Fig. 7: Force displacement curves (a) Green and cured samples with X-axis and 25 μm (b) Green and cured samples with Z-axis and 25 μm (c) Green and cured samples with X-axis and 50 μm (d) Green and cured samples with Z-axis and 50 μm .

3.1 Effect of Layer Thickness, Part Orientation, and Post-curing on Young's Modulus

In this part, a detailed explanation, supported by values and figures, is given of the relationship between the variables of the specimens manufacturing process with Young's modulus and manufacturing time. Where it will be explained:

1. Young's modulus vs. layer thickness for samples printed with X, 0° orientation & 25 μm , 50 μm thickness.
2. Young's Modulus vs. layer thickness for samples printed with Z, 90° orientation & 25 μm , 50 μm layer thickness.

Young's modulus vs. layer thickness for samples printed with X, 0° orientation & 25 μm , 50 μm thickness: for the green specimens, the average elastic modulus produced with layer thicknesses of 25 μm and 50 μm was 1301.961 MPa, 796.141 MPa, respectively. The modulus decreased clearly by 50.582% when layer thickness was increased from 25 μm to 50 μm . For cured samples, the average elastic modulus of the printed specimens with layer thicknesses of 25 μm and 50 μm was 1648.417 MPa and 1487.119 MPa, respectively. The modulus dropped by 16.13% when layer thickness was increased from 25 μm to 50 μm . In addition, the results imply that the elastic modulus increased with a thin layer, and that happens because of the resin's exponential decay in the amount of light it transmits, increased curing speeds along the layer, and increased adhesion between layers [26]. The data also showed that curing significantly increased elastic modulus, as the elastic modulus of a green specimen that was printed with a layer thickness of 25 μm grew to 1648.417 (34.6456 %) MPa when cured. Additionally, after curing, the elastic modulus of the green specimen, which was printed with a layer thickness of 50 μm (796.141 MPa), increased to 1487.119 MPa (69.09%). The elastic modulus of 25 μm samples was higher than that of 50 μm samples because they have a lower fraction of semi-reacted resin due to superior laser beam penetration through a thinner layer, see Fig. 8 (a) & (b).

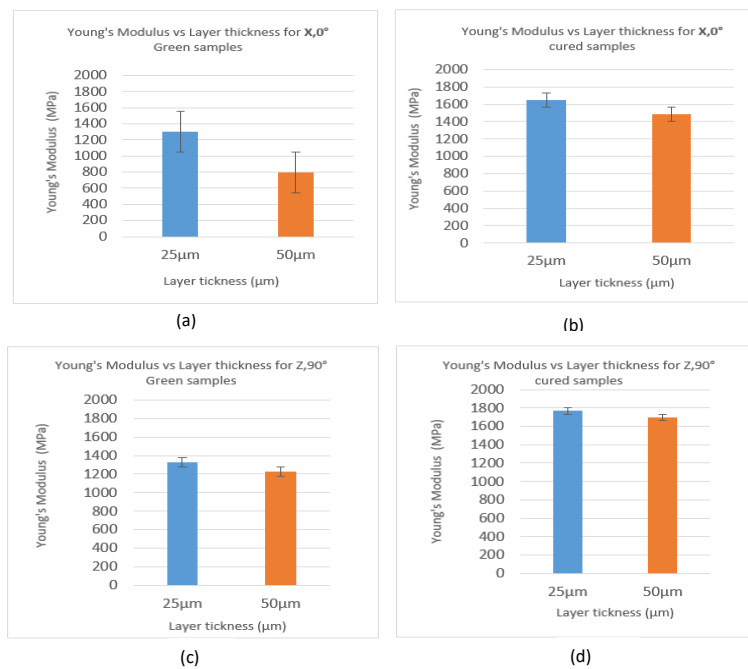


Fig. 8: Young's modulus vs. layer thickness for (a) X, 0° green samples (b) X, 0° cured samples (c) Z, 90° green samples (d) Z, 90° cured samples.

Young's Modulus vs. layer thickness for samples printed with Z, 90° orientation & 25 μm, 50 μm layer thickness: for green samples, the average elastic modulus for specimens produced with layer thicknesses of 25 μm and 50 μm was 1326.479 MPa and 1228.141 MPa, respectively. As can be seen, the modulus decreased by 9.8338 % when layer thickness was increased from 25 μm to 50 μm. For cured samples, the average elastic modulus of the specimens printed with layer thicknesses of 25 μm and 50 μm was 1767.274 MPa and 1699.033 MPa, respectively. As can be seen, the modulus dropped by 6.8241% when the layer thickness was increased from 25 μm to 50 μm. The elastic modulus of 25 μm samples was higher because they have a lower fraction of semi-reacted resin due to superior laser beam penetration through a thinner layer, see Fig. 8 (c) &(d). For green samples, the modulus of elasticity with X-direction and layer thickness varying from 50 and 25 μm increased from 796.141 to 1301.961 (increased 63.533%), and for the Z-direction increased from 1228.141 to 1326.479 MPa (increased 8%). For the cured sample, the modulus of elasticity with X-direction and layer thickness varying from 50 and 25 μm increased from 1487.119 to 1648.417 (increased 10.846%), and for Z-direction increased from 1699.033 to 1767.274 MPa (increased 4.016%). Therefore, the results showed that the modulus of elasticity with the X- direction is better than the Z-direction in both green and cured samples (see Fig. 9).

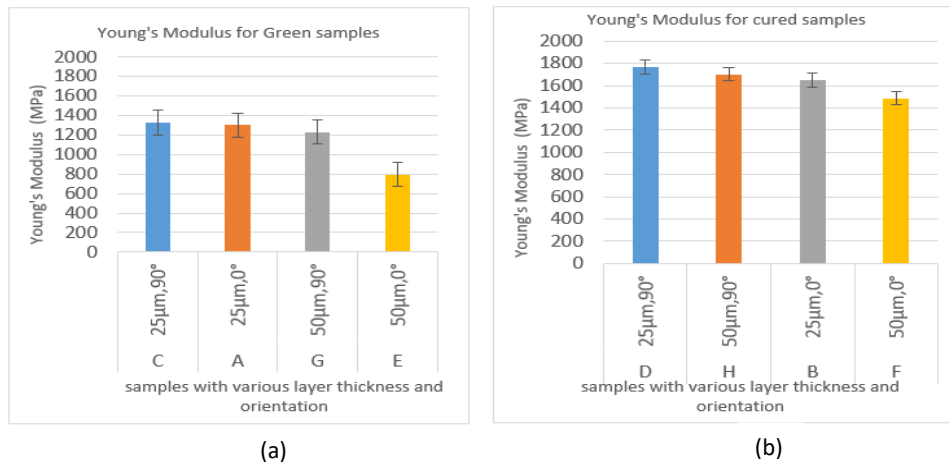


Fig. 9: Young's modulus for (a) Green samples (b) Cured samples.

Results showed that the thinner layer had higher elastic modulus, and that happened due to the exponential decay of light intensity transmission of the resin and getting higher curing rates along the layers and higher adhesion between layers.

3.2 Effect of Layer Thickness, Part Orientation, and Post-cure on Ultimate Stress

This part will explain the effect of the manufacturing process variables on the ultimate stress and printing time. Where it will be explained:

1. Ultimate stress vs. layer thickness for samples printed with X, 0° orientation & 25 μm, 50 μm thicknesses.
2. Ultimate stress vs. layer thickness for samples printed with Z, 90° orientation & 25 μm, 50 μm layer thicknesses.

Ultimate stress vs. layer thickness for samples printed with X, 0° orientation & 25 μm, 50 μm thicknesses: Figure 10 (c) & (d) demonstrates that specimens with the thinnest layer thickness can tolerate more stress than those with thicker layers. This outcome can be attributed to the resin transmittance, which allows a thinner layer to cure to a greater extent

than a thicker layer. For green samples, the average ultimate stress for specimens produced with layer thicknesses of 25 μm and 50 μm was 44.892 MPa, and 33.159 MPa, respectively. For cured samples, the average ultimate stress of the specimens printed with a layer thickness of 25 μm and 50 μm was 57.5566 MPa and 57.307 MPa, respectively.

Ultimate stress vs. layer thickness for samples printed with Z, 90° orientation, and 25 μm and 50 μm layer thickness: for green samples, the average ultimate stress for specimens produced with layer thicknesses of 25 μm and 50 μm was 49.217 MPa and 42.219 MPa, respectively. For cured samples, the average ultimate stress of the specimens printed with a layer thickness of 25 μm and 50 μm was 61.707 MPa and 60.277 MPa, respectively, see Fig. 10 (c) & (d).

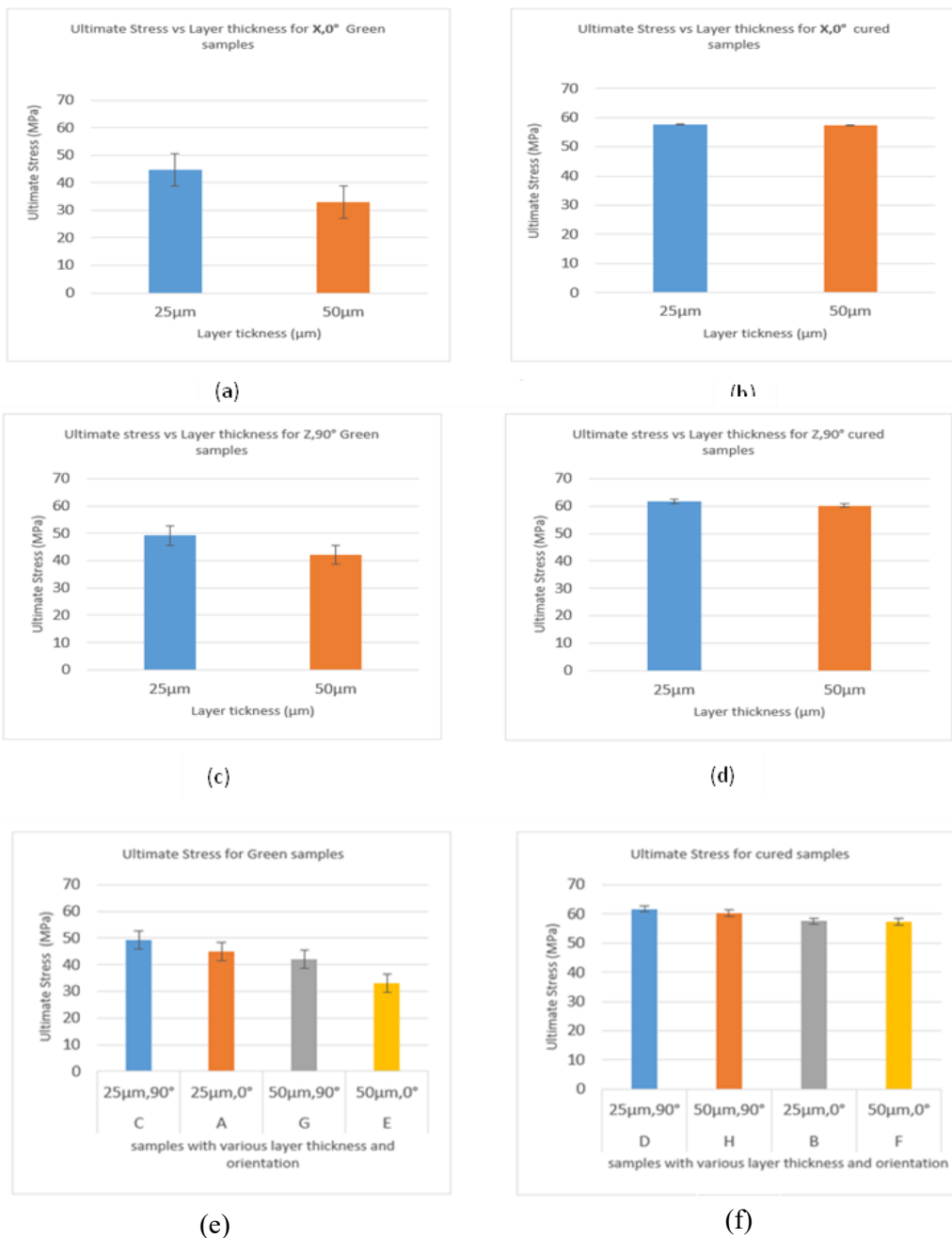


Fig. 10. Ultimate stress vs. layer thickness for (a) X, 0° green samples (b) X, 0° cured samples (c) Z, 90° green samples (d) Z, 90° cured samples (e) Green samples (f) Cured samples.

For green samples, the ultimate stress with X-direction and layer thickness varying from 50 and 25 μm increased from 33.159 to 44.892 (increased 35.384%), and for Z-direction increased from 42.219 to 49.217 MPa (increased 16.575%). For the cured sample, the ultimate stress with X-direction and layer thickness varying from 50 and 25 μm increased slightly from 57.307 to 57.556 (increased 0.004 %). For the Z-direction, it increased slightly from 60.277 to 61.707 MPa (increased by 2.372%). Therefore, the results showed that the ultimate stress with the X- direction is better than the Z-direction in both green and cured samples; see Fig. 10 (e) & (f).

The specimens with thin layers withstand greater forces than those with thicker layers, resulting from laser transmittance and providing a higher degree of curing to a thin layer than a thicker layer.

3.3 Effect of Layer Thickness, Part Orientation, and Post-cure on Ultimate Strain

The effect of manufacturing process variables on ultimate strain will be explained in this part. Where it will be explained:

1. Ultimate strain vs. layer thickness for samples printed with X, 0° orientation & 25 μm , 50 μm thickness.
2. Ultimate strain vs. layer thickness for samples printed with Z, 90° orientation & 25 μm , 50 μm layer thickness.

Ultimate strain vs. layer thickness for samples printed with X, 0° orientation & 25 μm , 50 μm thickness: for green samples, the average ultimate strain for specimens produced with layer thicknesses of 25 μm and 50 μm was 0.108 and 0.082, respectively. For cured samples, the average ultimate strain of the specimens printed with a layer thickness of 25 μm and 50 μm was 0.073 and 0.064, respectively, see Fig. 11(a) & (b).

Ultimate strain vs. layer thickness for samples printed with Z, 90° orientation & 25 μm , 50 μm layer thickness: for green samples, the average ultimate strain for specimens produced with layer thicknesses of 25 μm and 50 μm was 0.106, 0.103, respectively. For cured samples, the average ultimate strain of the specimens printed with a layer thickness of 25 μm and 50 μm was 0.0822 and 0.0815, respectively. By examining the results, the ultimate strain of the green samples was greater than that of the cured samples, see Fig. 11 (c) & (d). For green samples, the ultimate strain with X-direction and layer thickness varying from 50 and 25 μm increased from 0.0822 to 0.108 (increased 31.386%), and for Z-direction, increased from 0.103 to 0.106 MPa (increased 2.912%). For the cured sample, the ultimate strain with X-direction and layer thickness varying from 50 and 25 μm rose from 0.064 to 0.073 (increased 14.062%), and for Z-direction decreased from 0.081 to 0.067 MPa (fallen 20.895%). Therefore, the results showed that the ultimate strain with the X- direction is better than the Z-direction in both green and cured samples; see Fig. 11 (e) & (f).

4. CONCLUSIONS

In this study, the mechanical properties of 3D-printed photopolymers are examined and analyzed according to layer thickness, printing orientation, and post-curing. Based on the analyzed properties of elastic modulus, ultimate stress, and ultimate strain used to evaluate the printed samples, the results demonstrated that printing parameters significantly impacted mechanical properties. The results show that mechanical properties increased in X-orientation when the layer thickness varied from 50 to 25 μm in green printed samples. Therefore, the X-axis samples exhibit improvement in tensile strength and elastic modulus and have more elongation to failure when printed layers change to be thinner compared to

printed samples in the Z-axis. This could be due to the nature of the 3D printing procedure, which constructs a desired part layer-by-layer. When printing a new layer on the specimens, the additional UV-light exposure to previously printed layers will increase the polymerization of leftover unreacted monomers.

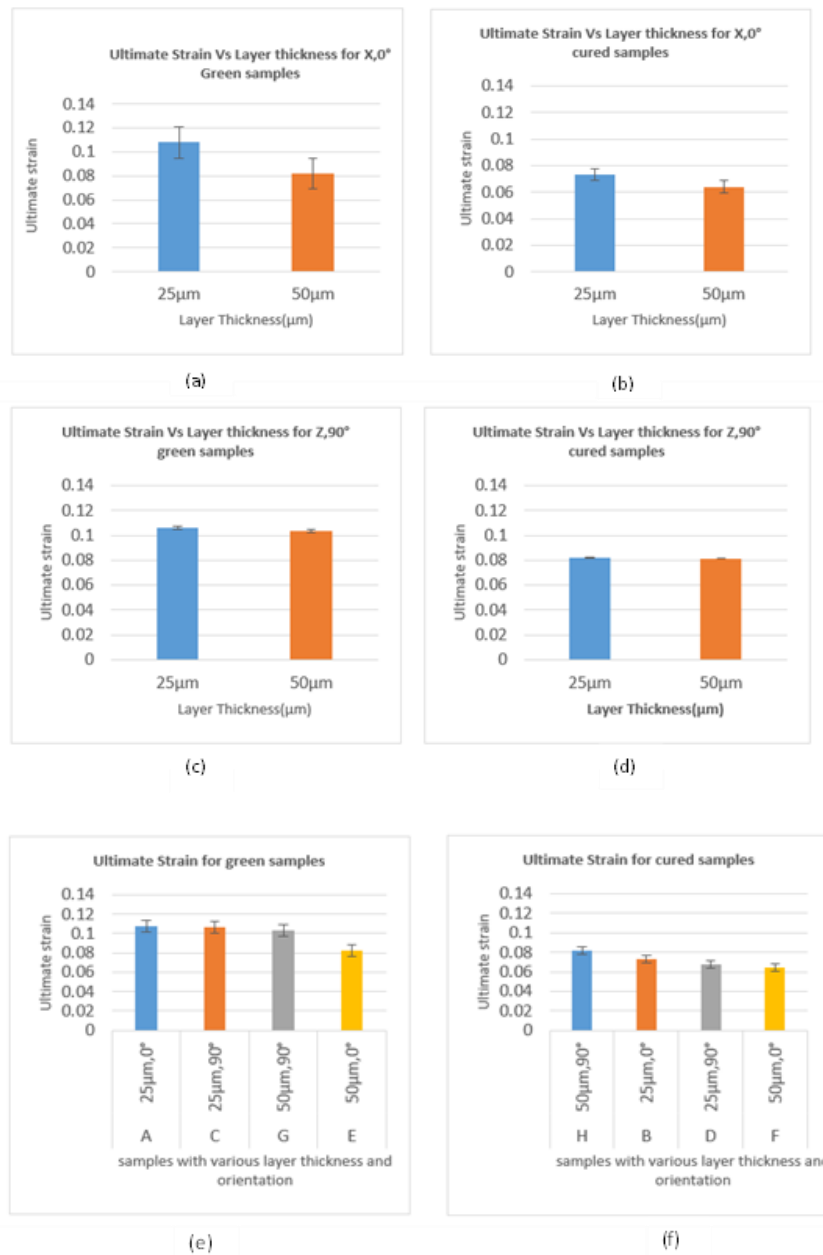


Fig. 11: Ultimate strain vs. layer thickness for (a) X, 0° green samples (b) X, 0° cured samples (c) Z, 90° green samples (d) Z, 90° cured samples (e) Green samples (f) Cured samples.

The interlayer fracture happens between the printed layers. In a thicker layer, the strength degraded faster in the specimen due to separation in the printed layers and increased interlayer stress. In contrast, the strength of specimens that are printed with a thin layer degraded slowly. Furthermore, in the case of vertical layer printing, the number of layers was large and thin. The laser-exposed surface area was large, enhancing the mechanical performance, which is distinct from horizontal printing.

The post-curing conditions had apparent effectiveness. UV curing under high temperatures and curing time improved the mechanical properties in both the X-axis and Z-axis and with various layer thicknesses. In the X- direction with 25 μm thickness, the elastic modulus increased by 26.61 % compared to the green samples. Also, the elastic modulus of the cured samples printed with 25 μm thickness and in the Z- direction increased by 33.23% compared to the green samples. The elastic modulus printed with 50 μm thickness and in the X-axis increased by 86.791% compared to the green samples. Also, the elastic modulus printed with 50 μm thickness and in the vertical direction increased by 38.341% compared to the green samples. In summary, there was an increase in ultimate stress values of the samples. For the ultimate strain, the green samples were generally higher than the cured samples, as the post-curing made the material behavior more brittle. According to the results obtained, the printing orientation, layer thickness, and post-curing of the build-direction of 3D printed samples play a role in improving and controlling the anisotropy of mechanical properties of the printed samples, which is considered a challenge that is faced in the additive manufacturing process.

REFERENCES

- [1] Ponce de Leon C, Hussey W, Frazao F, Jones D, Ruggeri E, Tzortzatos S, Mckerracher RD, Wills RGA, Yang S, Walsh FC. (2014) The 3D printing of a polymeric electrochemical cell body and its characterization. *Chemical Engineering Transactions*, 41: 1-6. <https://doi.org/10.3303/CET1441001>.
- [2] Chong S, Chiu HL, Liao YC, Hung ST, Pan GT. (2015) Cradle to Cradle® design for 3D printing. *Chemical Engineering*, 45. <https://doi.org/10.3303/CET1545279>.
- [3] Ngo TD, Kashani A, Imbalzano G, Nguyen KTQ, Hui D. (2018) Additive manufacturing (3D printing): A review of materials, methods, applications and challenges. *Composites Part B: Engineering*, 143: 172-196. <https://doi.org/10.1016/j.compositesb.2018.02.012>.
- [4] Standard, A.S.T.M. (2012) Standard terminology for additive manufacturing technologies. *ASTM International F2792-12a*, 1-9. <https://doi: 10.1520/F2792-12A>.
- [5] Hod L, Kurman M. (2013) *Fabricated: The new world of 3D printing*. John Wiley and Sons, 2013.
- [6] Ivanova O, Williams C, Campbell T. (2013) Additive manufacturing (AM) and nanotechnology: promises and challenges. *Rapid prototyping journal*, 19 (5): 353-364. <https://doi.org/10.1108/RPJ-12-2011-0127>.
- [7] Quan Z, Wu A, Keefe M, Qin X, Yu J, Suhr J, Byun JH, Kim BS, Chou TW. (2015) Additive manufacturing of multi-directional preforms for composites: opportunities and challenges. *Materials Today*, 18 (9): 503-512. <https://doi.org/10.1016/j.mtadv.2019.100045>.
- [8] Quan Z, Larimore Z, Wu A, Yu J , Qin X, Mirotznik M, Suhr J, Byun JH, Oh Y, Chou TW. (2016) Microstructural design and additive manufacturing and characterization of 3D orthogonal short carbon fiber/acrylonitrile-butadiene-styrene preform and composite. *Composites Science and Technology*, 126:139-148. <https://doi.org/10.1016/j.compscitech.2016.02.021>.
- [9] Skliutas E, Kasetaitė S, Jonušauskas L, Ostrauskaite J, Malinauska M. (2018) Photosensitive naturally derived resins toward optical 3-D printing. *Optical Engineering*, 57(4): 041412-041412. <https://doi.org/10.1117/1.OE.57.4.041412>.
- [10] Januszewicz R, Tumbleston JR, Quintanilla AL, Mecham SJ, DeSimone JM. (2016) Layerless fabrication with continuous liquid interface production. *Proceedings of the National Academy of Sciences*. 113(42): 11703-11708. <https://doi.org/10.1073/pnas.1605271113>.
- [11] O'Neil PF. (2018) Internal void fabrication via mask projection micro-stereolithography: a rapid repeatable microfluidic prototyping technique. Ph.D Dissertation. Dublin City University, 2018.

- [12] Naik D, Kiran R. (2018). On Anisotropy, Strain Rate and Size Effects in Vat Photopolymerization Based Specimens. *Additive Manufacturing*, 23: 181-196. <https://doi.org/10.1016/j.addma.2018.08.021>.
- [13] E Aznarte, Ayranci C, Qureshi AJ. (2017) Digital light processing (DLP): Anisotropic tensile considerations. 2017 International Solid Freeform Fabrication Symposium. University of Texas at Austin.
- [15] Agrawal S, Ray H, Kulat A, Garhekar Y, Jibhakate R, Singh S, Bisaria H. (2023) Evaluation of Tensile Property of SLA 3D Printed NextDent Biocompatible Class I Material for Making Surgical Guides for Implant Surgery. *Materials Today: Proceedings*, 72: 1231-1235. <https://doi.org/10.1016/j.matpr.2022.09.288>.
- [16] Lee CS, Kim SG, Kim HJ, Ahn SH. (2007) Measurement of Anisotropic Compressive Strength of Rapid Prototyping Parts. *Journal of materials processing technology*, 187: 627-630. <https://doi.org/10.1016/j.jmatprotec.2006.11.095>.
- [17] SH. Ahn, M. Montero, D. Odell, S. Roundy, and P. Wright. (2002) Anisotropic Material Properties of Pused Deposition Modeling ABS. *Rapid prototyping journal*, 8: 248-257. <https://doi.org/10.1108/13552540210441166>.
- [18] Mueller J, Shea K, and Daraio C. (2015) Mechanical Properties of Parts Fabricated with Inkjet 3D Printing Through Efficient Experimental Design. *Materials and Design*, 86: 902-912. <https://doi.org/10.1016/j.matdes.2015.07.129>.
- [19] Chockalingam K, Jawahar N, Chandrasekhar U. (2006) Influence of Layer Thickness on Mechanical Properties in Stereolithography. *Rapid Prototyping Journal*, 12: 106-113. <https://doi.org/10.1108/13552540610652456>.
- [20] Rankouhi B, Javadpour S, Delfanian F, Letcher T. (2016) Failure Analysis and Mechanical Characterization of 3D Printed ABS with Respect to Layer Thickness and Orientation. *Journal of Failure Analysis and Prevention*, 16 :467-481. <https://doi.org/10.1007/s11668-016-0113-2>.
- [21] Quintana R, Choi JW, Puebla K, Wicker R. (2010) Effects of Build Orientation on Tensile Strength for Stereolithography-Manufactured ASTM D-638 Type I Specimens. *The International Journal of Advanced Manufacturing Technolog*, 46: 201-215. <https://doi.org/10.1007/s00170-009-2066-z>.
- [22] Domínguez-Rodríguez G, Ku-Herrera J, Hernández-Pérez A. (2018) An Assessment of the Effect of Printing Orientation, Density, and Filler Pattern on the Compressive Performance of 3D Printed ABS Structures by Fuse Deposition. *The International Journal of Advanced Manufacturing Technology*, 95: 1685-1695. <https://doi.org/10.1007/s00170-017-1314-x>.
- [23] Rohde S, Cantrell J, Jerez A, Kroese C, Damiani D, Gurnani R, DiSandro L, Anton J, Young A, Steinbach D, Ifju P. (2018) Experimental Characterization of The Shear Properties of 3D-Printed ABS and Polycarbonate Parts. *Experimental Mechanics*, 58: 871-884. <https://doi.org/10.1007/s11340-017-0343-6>.
- [24] Zguris Z. (2016) How Mechanical Properties of Stereolithography 3D Prints are Affected by UV Curing. *Formlabs White Paper*, 1-11.
- [25] Kerns J. (2015) What's the difference between stereolithography and selective laser sintering. *Machine Design*, 17.
- [26] ASTM International (2014) Standard test method for tensile properties of plastics. ASTM international.